

Particle-laden viscous thin-film flows on an incline: experiments compared with an equilibrium theory

N. Murisic^a, J. Ho^b, V. Hu^c, P. Latterman^d, T. Koch^e, K. Lin^f, M. Mata^a, A. Bertozzi^a

^aMathematics Department, University of California, Los Angeles, CA 90095, USA

^bDepartment of Chemical and Biomolecular Engineering, University of California, Los Angeles, CA 90095, USA

^cMechanical and Aerospace Engineering Department, University of California, Los Angeles, CA 90095, USA

^dDepartment of Bioengineering, University of California, Los Angeles, CA 90095, USA

^eDepartment of Physics, Harvey Mudd College, Claremont, CA 91711, USA

^fDepartment of Mathematics, The University of Hong Kong, Pokfulam, Hong Kong

Abstract

We consider gravity driven flows of particle-laden thin films on an incline. Three distinct regimes are observed depending on the inclination angle and the bulk volume fraction of particles: the particles either settle out of the flow, aggregate at the moving front, or remain well-mixed. The experiments are carried out with a range of particle sizes and fluid viscosities. The results compare well with an equilibrium theory balancing shear-induced migration with settling in the normal direction. We find that the well-mixed regime is transient in nature, with both the particle size and the liquid viscosity affecting the time scale on which it occurs.

Key words: thin films, particle-laden flows, fingering instability, shear-induced migration

PACS: 47.15.gm, 47.55.Kf, 83.80.Hj

1. Introduction and background

Particle-laden flows in general are important in a variety of contexts, including environmental, industrial and biological ones, where transport and manipulation of suspensions occur. Specific examples are mud flows, debris flows, slurry transport, food processing, various coating processes in ceramics and electronics industries, and manufacturing processes in pharmaceutical and paper industries, where uniformity in particle distribution is usually required. While many studies in the literature address gravity-driven clear liquid flows (e.g. see [1, 2, 3, 4, 5, 6]) and pure granular flows (e.g. [7, 8, 9]), comparatively fewer studies have centered on particle-laden thin film flows [10, 11, 12, 13]. Apart from complexities associated with moving contact lines, the study of slurries also involves an intricate interplay between particle settling/migration and viscous fingering mechanisms.

1.1. Settling of particles due to gravity

The settling of particles in quiescent liquids and sedimentation in suspensions have also garnered significant attention (e.g. see [14, 15, 16, 17, 18, 19]). For rigid spherical particles, the well-known Stokes' Law applies, neglecting inertial effects of the liquid due to the smallness of Reynolds number. In order to account for the presence of a large number of identical particles, the velocity given by Stokes' Law is typically modified by a purely empirical multiplicative hindrance function which depends on particle volume fraction, ϕ . This function, typically denoted by $f(\phi)$, has been a matter of much discussion through the decades. In [14], a so-called Richardson-Zaki expression was proposed, where $f(\phi) \sim (1 - \phi)^m$, with $m \approx 5.1$, and found

to compare favorably with experimental data for moderately dilute suspensions. For dilute dispersions, $f(\phi) \sim (1 - 6.55\phi)$ was suggested in [15]. Other, more complex expressions for $f(\phi)$ were discussed in [16, 17, 18] and [19]. In the presence of shear, a hindrance function of form $f(\phi) \sim (1 - \phi)$ was shown to be appropriate in [20].

1.2. Shear-induced migration of particles

Concentrated suspensions of spherical particles have been shown to behave curiously when subjected to shear. This phenomena was first detected in experiments with Couette viscometer, where unusual decrease in measured viscosity occurred during prolonged shearing. The theoretical framework for this phenomena was laid out in [21, 22] and subsequently rephrased in [23]. Its key element was *shear-induced migration*, a diffusive mechanism resulting from gradients in both particle volume fraction and suspension viscosity, $\mu(\phi)$. Net fluxes caused by these gradients were deduced by considering irreversible interactions between pairs of smooth spherical particles (for details, see [22]). In [23], the predictions of this model were shown to be in excellent agreement with experimental data for Couette flows, and the use of the model was also extended to flows of concentrated suspensions through cylindrical tubes. Recently, the model was employed in [24] to carry out numerical simulations for suspension flows in more complex geometries. Other studies, focusing on migration of particles in pressure-driven channel flows [25], steady and unsteady flows in various geometries [26], and inclined free-surface channel flows [27], were carried out using a different approach, based on Stokesian Dynamics.

1.3. Particle-laden thin film flows

More recent studies addressed particle-laden thin film flows with contact lines. Zhou *et. al* [10] reported on their preliminary experimental results for incline flows of suspensions of polydisperse glass beads with diameter $\sim O(100\mu\text{m})$, focusing on a single bead size. As they varied the bulk particle volume fraction, ϕ_0 , and the inclination angle, α , they identified three distinct settling regimes: for small ϕ_0 and α values, the particles would settle out of the flow, clear liquid film would flow over the particulate bed and the fingering instability resulted; for large values of ϕ_0 and α , the particles would move faster than the liquid, leading to aggregation of particles in the contact line region, formation of particle-rich ridge, and almost complete suppression of the fingering instability; finally, intermediate values of these parameters would lead to a well-mixed regime in which fingering instability occurred. A theoretical model was also derived in [10], based on the Navier-Stokes equations for the liquid and a diffusive model for particle volume fraction, including capillary effects and hindered settling. A simplified version of this model, which neglected higher order capillary terms was studied in a shock dynamics framework in [10] and [11]. Although successful in explaining qualitatively the formation of the particle-rich ridge, they did not provide a quantitative model nor did they ever attempt to model the other regimes. In an effort to improve understanding of these regimes, Cook [12] included shear-induced migration in his model. He assumed that the outcome of particle settling is guided by the balance between shear-induced migration and hindered settling. Through his steady state formulation, he derived a system of ODEs for ϕ and shear stress, σ . However, this model did not include a significant hindrance effect due to the presence of the solid track. Furthermore, while he found good agreement between model's predictions regarding well-mixed regime and the experimental data, the data itself was from [10] – old, preliminary and rather limited. Additional work in [13] focused on studying the propagation of contact lines in particle-laden thin film flows experimentally. Apart from varying ϕ_0 and α , particle size and density, and liquid viscosity were all varied in order to examine their influence on the front speed. It was found that the dependence of the front position on time was of power-law type, with exponents similar to $1/3$ proposed in [1].

1.4. The objectives

In this work we carry out a systematic study of settling regimes over a range of particle sizes and liquid viscosities. Through comparison between our experimental results and the predictions of equilibrium theory, we uncover the transient nature of the well-mixed regime, where bifurcation to either of the remaining regimes eventually occurs. In addition, our experimental results clearly indicate how the particle size and the liquid viscosity affect the time scale on which we observe this transient regime.

In contrast to the preliminary experimental results from [10], we perform experiments with three different particle sizes and two different liquid types, and vary ϕ_0 and α over wide ranges of values. The liquid viscosity and the particle size are found

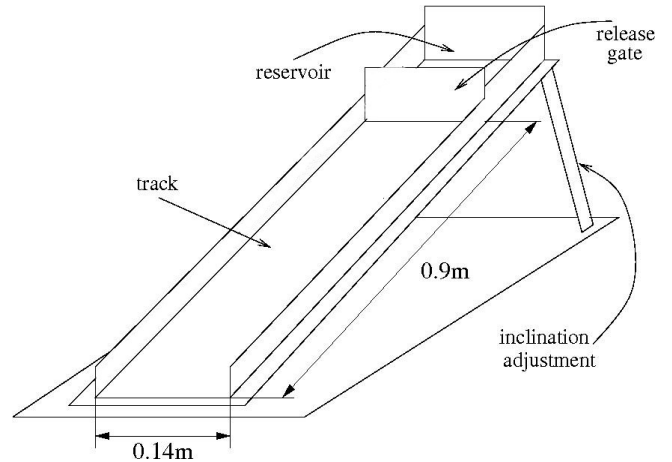


Figure 1: The experimental apparatus.

to affect the width of the region in (ϕ_0, α) -space over which the transition between settled and ridged regimes occurs. Therefore, we show that these parameters dictate both the likelihood of observing the well-mixed regime for given ϕ_0 and α values, and the time scale over which the well-mixed suspension is preserved. Next, a theoretical model is derived. We consider the steady state of the system where hindered settling balances the shear-induced migration of particles. Our modeling approach is similar to the one in [12], with one important difference: we also include the hindrance to settling due to the presence of the solid track. We proceed by showing excellent agreement between model's predictions and our experimental results over all ranges of viscosities and particle sizes. Furthermore, we show how the results of numerical simulations of our model provide additional evidence for transiency of well-mixed regime.

This paper is organized as follows. In §2 we describe our experimental set-up, list material parameters and identify the techniques employed in collecting data. This is followed by a discussion of our experimental results in §3, and the outline of the derivation of our theoretical model in §4. In §5, we compare the predictions of our model with the experimental results. Finally, we summarize our findings and discuss challenges in going from equilibrium to full dynamic theory in Conclusions.

2. Experimental apparatus and techniques

Figure 1 shows the experimental apparatus we use. It consists of a steel base platform and an acrylic track, with adjustable inclination angle, α (range: $5^\circ - 80^\circ$). The track is 0.9 m long and 0.14 m wide, with 0.02 m side walls. A liquid/particle mixture prepared beforehand is poured into the reservoir situated at the top of the track and the gate is lifted, allowing it to flow down the track, with the contact line initially straight. Here, we only focus on experiments with finite, constant suspension volume. The evolution of the flow is monitored using a digital camera, which is positioned above the track and

	ν (m^2/s)	ρ_l (kg/m^3)	ρ_p (kg/m^3)	d (mm)
L1	10^{-4}	966	–	–
L2	10^{-3}	971	–	–
P1	–	–	2475	0.143
P2	–	–	2475	0.337
P3	–	–	2475	0.625

Table 1: Physical properties of liquids and particles used in the experiments.

captures images of the moving front at predetermined time intervals, typically $0.25 - 4$ s. Using this setup, we are able to monitor the film motion, starting from release, until the front has reached approximately 0.6 m down the track. Several fluorescent lights are placed below the track for imaging purposes, while food-coloring dye is employed to enhance contrast. Images are subsequently analyzed, and each experimental run is classified, based on observed settling regime, as either ‘settled’, ‘well-mixed’ or ‘ridged’ (see §3 for details).

Our experiments involve three different particle types and two different liquids. The particles are smooth spherical glass beads (Ceroglass), and we consider three different diameters: $d = 0.143$ mm (‘P1’), 0.337 mm (‘P2’), and 0.625 mm (‘P3’). The standard deviation of particle diameters is 26% for all particle sizes. For suspending liquid, we use polydimethylsiloxane (PDMS) (AlfaAesar) in two different kinematic viscosities: $\nu = 10^{-4}$ m^2/s (‘L1’) and 10^{-3} m^2/s (‘L2’). The particles are heavy, i.e. $\rho_p > \rho_l$ for all particle and liquid types, where ρ_p and ρ_l are particle and liquid densities respectively. Relevant material parameters are summarized in Table 1.

Suspensions are prepared by first weighing the particles and PDMS individually, pouring PDMS into a container, and then adding particles; slow manual stirring is used until uniform mixture is obtained. This procedure prevents formation of air bubbles. Typically, no haste is required between the preparation of suspension and its release down the track since uniformity of the mixture is preserved for sufficiently long time-intervals. The bulk volume fraction of particles, ϕ_0 , is defined as $\phi_0 = V_p/V$, where $V = V_l + V_p$ is the total volume of the mixture, and V_l and V_p are liquid and particles volumes respectively. Here, we focus on V between 75 ml and 103 ml.

The experiments are carried out in open air and at room temperature (298 K), maintained by the air-conditioning unit. The fluorescent lights we use for imaging purposes radiate heat, but the amount is insufficient to affect either viscosity of liquid, flow dynamics, or observed particle behavior in any significant manner. The track, gate and reservoir are cleaned after each experimental run using a squeegee to remove the excess particulate and dust which may accumulate. Although this cleaning procedure does not remove PDMS entirely, it ensures reproducibility of our experimental results.

We carry out three different sets of experiments, conveniently summarized in Table 2. In all experiments, we vary ϕ_0 between 0.25 and 0.50 , and α between 20° and 50° . In Experiment A, we consider medium-sized particles, P2, and both PDMS types in order to study the influence of the viscosity of suspending liquid

	P1	P2	P3
L1	Experiment C	Experiments A,C	–
L2	Experiment B	Experiments A,B	Experiment B

Table 2: Different liquid/particle combinations we consider. We study the manner in which viscosity of suspending liquid (Experiment A) or particle size (Experiments B and C) affects the settling regime.

of the settling regime. Experiments B and C focus on studying the influence of particle size, by fixing the liquid type (L2 in B and L1 in C) and varying the particle size. When L1 PDMS and P3 particles are used, rapid settling occurs. Regardless of our best efforts, significant fraction of particles often settles to the bottom of the reservoir before suspension is ever released down the track. Hence, we omit experiments with this mixture.

3. Experimental results

In all experiments, the observed flows are relatively slow. In addition, settling behavior can only be classified after an initial transient stage which typically lasts up to 900 s. The settling regimes observed in our experiments resemble the ones discussed in [10]: each experimental run is labeled as either settled, well-mixed, or ridged. Typical examples of these regimes are shown in Fig. 2. In general, these three regimes occur in each experimental set, A, B and C (an exception is discussed below).

In settled regime, the particles tend to quickly settle out of the flow, forming a particulate bed, with the suspending liquid moving down the track faster than particles. Virtually clear liquid film ultimately leaves the particulate bed far behind and develops the fingering instability as described in [1]. Typically, this regime occurs for small values of ϕ_0 and α . In contrast, when ϕ_0 and α are large, the particles move faster than suspending liquid, they aggregate in the contact line region, forming a particle-rich ridge, often several times thicker than trailing film. Hence, we refer to this regime as ridged. Large volume fraction of particles at the front appears to suppress the fingering instability. Intermediate values of ϕ_0 and α lead to well-mixed regime, where volume fraction of particles remains almost uniform throughout the film. The fingering instability occurs, but compared to settled regime, it is typically characterized by longer wavelength.

For any particular liquid/particle combination, we classify each experimental run and compile the results of the classification in a corresponding (ϕ_0, α) phase diagram (see Figs. 3, 4 and 5). Same-type settling behaviors cluster in these diagrams, forming distinct bands. We use color to label these regime bands: *white* for settled, *light* for well-mixed, and *dark* for ridged. Figures 3, 4 and 5 each include a curve superposed on the experimental results. These curves represent a well-mixed regime prediction (i.e. $\phi' = 0$, where $\phi(z)$ is particle volume fraction) of our theoretical model. The discussion regarding the model and the agreement between its predictions and the experimental results is given in §4 and 5.

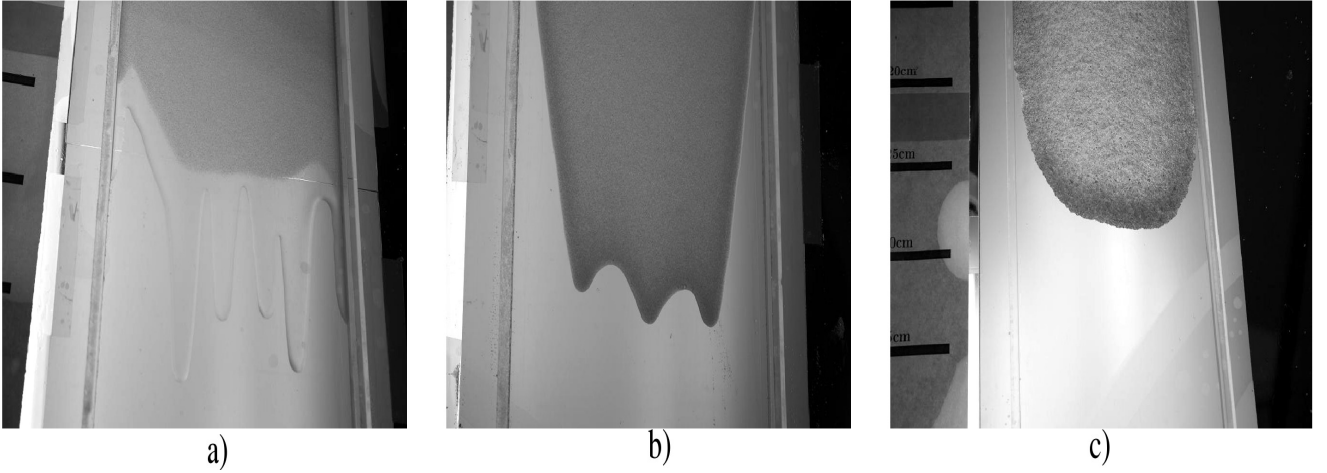


Figure 2: The settling regimes: a) settled; b) well-mixed; and c) ridged. The fingering instability typical to clear liquid flows is *only* observed in settled and well-mixed regimes.

We note that other more complex behavior also occurs. In some experimental runs, we notice capillary motion of particles along the side walls or their alignment in linear streaks along the track. Irregularities in shape and size of fingers, and extreme cases of ridged regime, where sections of contact line experience jamming with particles, become solid-like and virtually break off in blocks are also observed. These phenomena are attributed to either finite width of track and presence of side walls or complex interplay between particle migration and contact line effects. While very intriguing, we leave detailed study of such complex behavior for future work, and focus here on three settling regimes described above.

We proceed by discussing dependence of settling behavior on viscosity of suspending liquid and particle size by presenting results of Experiments A, B and C.

3.1. Experiment A: influence of viscosity of suspending liquid

In Experiment A, we consider intermediate size particles, P2, and both the low and the high viscosity liquid (L1 and L2 respectively). This allows us to study the dependence of observed settling behavior on PDMS viscosity. Since, based on Stokes' Law (e.g. see [15]), the settling velocity of particles is inversely proportional to liquid viscosity, a decrease in PDMS viscosity should result in enhanced tendency of particles to settle out of the flow. Figure 3 shows phase diagrams which result for low (a) and high viscosity (b)).

At a first glance, the outcomes appear to be rather similar for the two liquids, although the band for the settled regime is somewhat wider in Fig. 3a) compared to b), confirming our expectations based on the settling time. A closer inspection also reveals that the well-mixed band is noticeably wider when the viscosity of the suspending liquid is lower (Fig. 3a)). In order to better understand this difference, we consider the time scales of the motion of the front and the settling of the particles. For clear liquid inclined flows, the former time scale is proportional to the viscosity of the liquid (e.g. see [10]), $T \propto \mu$. However, for suspensions $\mu = \mu(\phi)$. For estimation purposes, we may

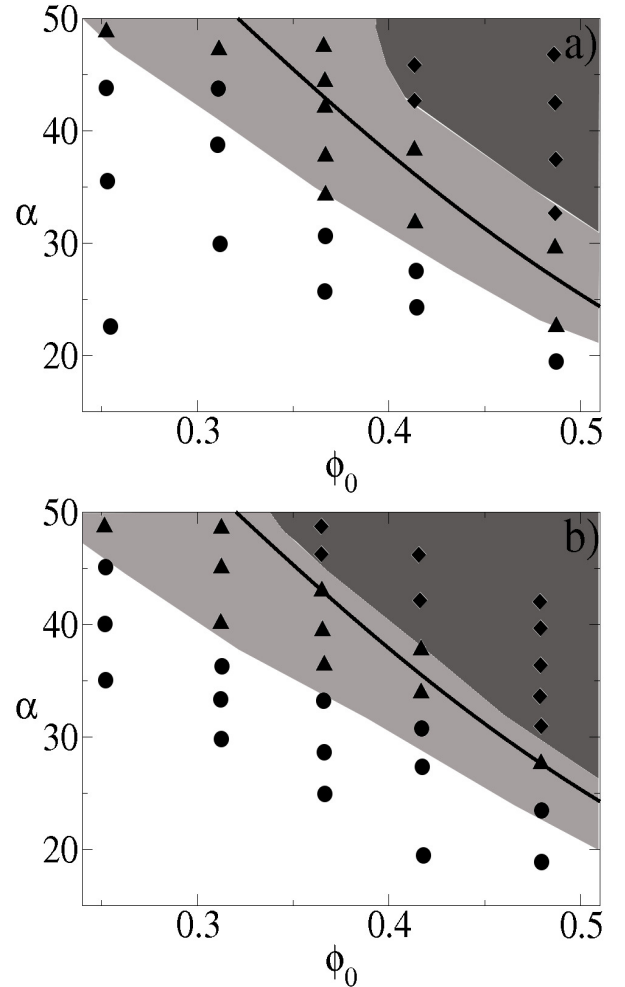


Figure 3: Phase diagrams for Experiment A. Particle type is fixed (P2), viscosity of suspending liquid is varied: a) low (L1); and b) high (L2). Symbols denote regimes observed in experimental runs: circles (●) for settled, triangles (▲) for well-mixed, and diamonds (◆) for ridged. The solid curve represents prediction of our theoretical model (see §4 and 5) for a regime where $\phi' = 0$ (well-mixed).

assume uniformity of the slurry (i.e. well-mixed case), and by using $\mu = \rho_l \nu (1 - \phi/\phi_{max})^{-2}$ as in [27], we get that $T \propto \nu$. It is now clear that a decrease in the viscosity of the suspending liquid, with all the other material parameters fixed, leads to a faster propagation of the suspension front. On the other hand, for purely gravity driven particle settling, the relevant time scale is viscous and also directly proportional to ν (see §4) – a decrease in viscosity leads to a faster settling of particles. Therefore, if gravity were the only mechanism responsible for particle settling, the width of the well-mixed bands in Fig. 3 would have been independent of the viscosity. The fact it is not, suggests that some part of the relevant settling dynamics occurs on a time scale other than the viscous one. In §4, we conjecture that the settling behavior is governed by a balance between the settling due to gravity and the shear-induced migration. This balance may lead to a settling which occurs on a different time scale, introducing a correction to the pure viscous one. Accordingly, while a decrease in the viscosity clearly affects the motion of the front, it may only have a relatively minor effect on the settling rate. Hence, due to the finite length of the track used in the experiments, the suspensions with low viscosity PDMS are likely to run out of track length before the final state of the system has been achieved. As a result, some runs which, given a longer track, would eventually become settled or ridged, are classified as well-mixed. This argument not only explains the differences between Figs. 3a) and b), but also gives a hint regarding the nature of the well-mixed regime: it appears to be an intermediate transient state of the system that eventually, given a sufficient time, bifurcates to either the settled or the ridged regime. The notion of transiency of well-mixed regime is revisited throughout this section and in §5.

3.2. Experiments B and C: influence of particle size

Next, we examine the manner in which particle size affects the settling regime. For this purpose, we carry out Experiments B and C, where liquid type is fixed and particle size is varied.

In Experiment B, we consider high viscosity suspending liquid, L2, and all three particle sizes, P1, P2, and P3 (note: experimental runs with L2/P2 combination have already been carried out in Experiment A). According to Stokes' Law, the settling velocity is proportional to d^2 , and hence, largest particles are most likely settle out of the flow. Based on this reasoning, the settled band should be widest for P3. The phase diagrams resulting from Experiment B are shown in Fig. 4.

Compared to Experiment A, the differences between different diagrams are much more pronounced. The speculation based on Stokes' Law is again proven correct – compared to Figs. 4a) and b), the band corresponding to settled regime is widest in Fig. 4c); it is narrowest for smallest particles in Fig. 4a). But, the most striking feature here is a complete absence of well-mixed regime for largest particles in Fig. 4c) – all considered runs with L2/P3 configuration resulted in either settled or ridged behavior. In addition, we notice that the well-mixed band is significantly wider for smallest particles in Fig. 4a) compared to intermediate ones in Fig. 4b). Hence, the trend is obvious: for a fixed liquid viscosity, an increase in particle size makes the well-mixed outcome less likely. This result

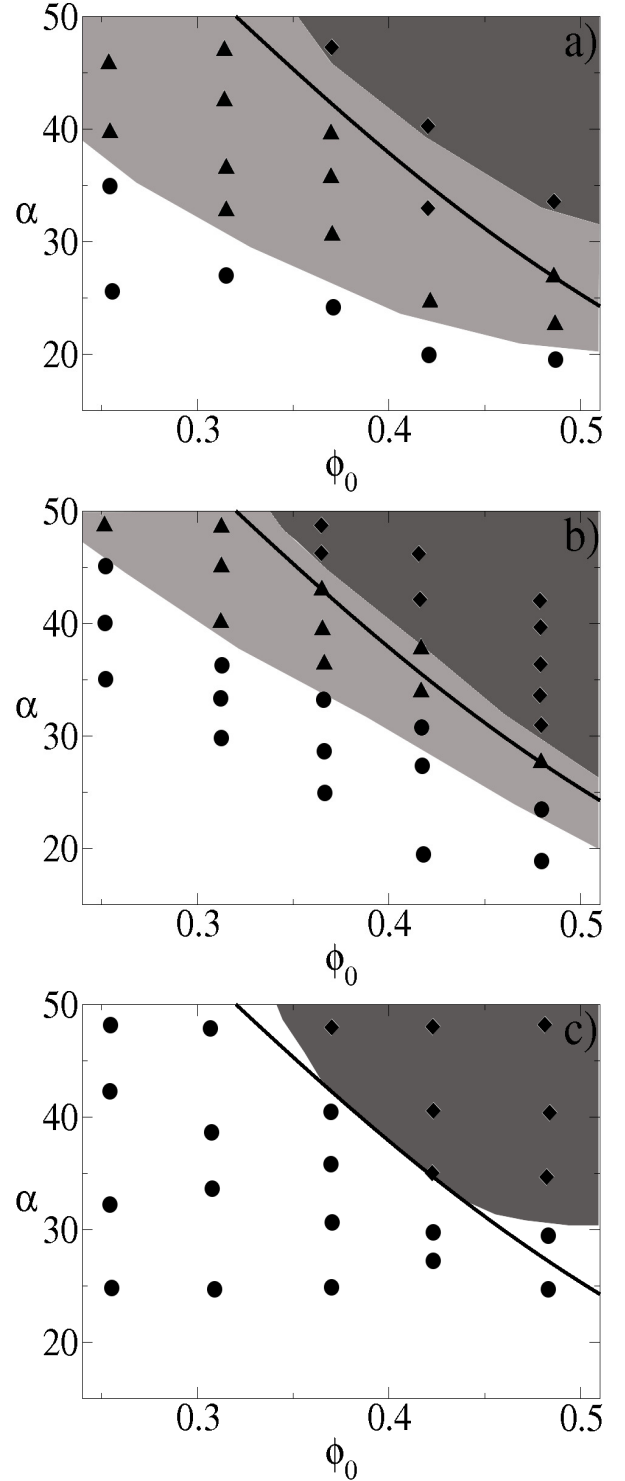


Figure 4: Phase diagrams for Experiment B. Viscosity of suspending liquid is fixed (high viscosity, L2), particle size is varied: a) small (P1); b) intermediate (P2); and c) large (P3). Symbols denote regimes observed in experimental runs: circles (●) for settled, triangles (▲) for well-mixed, and diamonds (◆) for ridged. The solid curve represents prediction of our theoretical model (see §4 and 5) for a regime where $\phi' = 0$ (well-mixed).

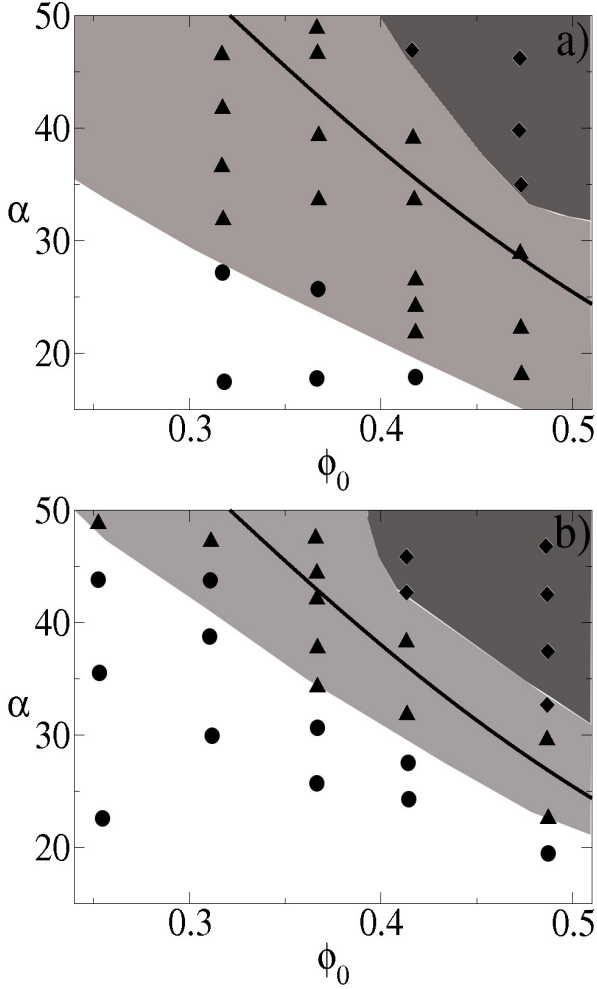


Figure 5: Phase diagrams for Experiment C. Viscosity of suspending liquid is fixed (low viscosity, L1), particle size is varied: a) small (P1) and b) intermediate (P2). Symbols denote regimes observed in experimental runs: circles (●) for settled, triangles (▲) for well-mixed, and diamonds (◆) for ridged. The solid curve represents prediction of our theoretical model (see §4 and 5) for a regime where $\phi' = 0$ (well-mixed).

further supports our hypothesis regarding the transient nature of well-mixed regime. In particular, the diffusive fluxes of particles due to hindered settling and shear-induced migration are both proportional to d^2 (see §4). Since these are, in our opinion, the two main mechanisms of particle motion in the system we study, the smallest particles P1 are moving on a time scale much longer than larger particles P2 and P3. Consequently, and as seen in Fig. 4a), many runs involving P1 remain well-mixed for the duration of the experiment. We suspect that given a longer track and larger sample volume, majority of these flows would eventually bifurcate to either settled or ridged regime. On the other hand, the largest particles P3 move on shorter time scale compared to both P1 and P2. Therefore, the flows involving particles P3 quickly bifurcate to either settled or ridged, with latter regime likely for most ϕ_0 and α values. The complete absence of well-mixed band in Fig. 4c) serves as an indicator of just how rapid this process is.

Finally, in Experiment C, we study the influence of parti-

cle size on the settling behavior for low viscosity PDMS, L1. We focus on small and intermediate size particles, P1 and P2. As discussed in §2, we do not consider the L1/P3 combination since particles in all suspensions of that type undergo rapid settling while still in the reservoir. We also note that runs with the L1/P2 combination have already been carried out in Experiment A.

The results of Experiment C are shown in Fig. 5. The trend observed in Experiment B is very much noticeable here too: as the particle size increases, the uniformity of the suspension is less likely to be preserved. In particular, the well-mixed band is significantly wider in Fig. 5a) compared to the one in b) for larger particles. The explanation for this trend is identical to one for Experiment B. For small particles, the time scale of particle settling is much longer than for larger ones; therefore, uniformity of suspension is likely to be preserved longer for small particles. Furthermore, a comparison of diagrams in Figs. 3, 4 and 5 reveals that the well-mixed regime is more likely to occur for L1/P1 than for any other liquid/particle combination we consider – the well-mixed band in Fig. 5a) is by far the widest. This is particularly evident when Figs. 4a) and 5a) are compared (small particle size, high and low viscosity suspending liquid respectively). The latter comparison also shows that for smallest particles, the influence of viscosity on both prolonging the transient phase and making it more likely for wider range of ϕ_0 and α values is much more pronounced than in Experiment A.

To summarize, Experiments A, B and C show that particle size particularly affects the settling behavior. It dictates the likelihood of occurrence of settled regime and the time scale for particle-motion in general. The viscosity of the suspending liquid also influences the particles motion, and increasingly so for smaller particles. The experiments also reveal the transient nature of the well-mixed regime. This is evident from the manner in which both particle size and viscosity of the suspending liquid affect the persistence of the well-mixed regime. We argue that given a longer track length, a majority of, if not all, well-mixed flows would bifurcate to either the settled or the ridged regime. We revisit this argument again when we compare the predictions of our theoretical model and the experimental results in §5.

4. Theoretical model

We consider a continuum model for particle volume fraction, ϕ . The dynamics of ϕ are described by a conservation equation for particles, written in Eulerian reference frame

$$\frac{D\phi}{Dt} = -\nabla \cdot (\mathbf{J}_{bd} + \mathbf{J}_{grav} + \mathbf{J}_{coll} + \mathbf{J}_{visc}). \quad (1)$$

Here t denotes time, and $D/Dt = \partial/\partial t + \mathbf{v} \cdot \nabla$, where $\mathbf{v} = (\mathbf{u}, \mathbf{w})$; u and w are components of liquid velocity vector \mathbf{v} in x -direction (down the track) and z -direction (normal to track) respectively. Equation 1 includes hindered settling (\mathbf{J}_{grav}), and shear-induced migration effects (\mathbf{J}_{coll} and \mathbf{J}_{visc}). It also includes Brownian diffusive flux, $\mathbf{J}_{bd} = -D\nabla\phi$. We note that since the Péclet number corresponding to our problem is small (i.e. $Pe = \dot{\gamma}d^2/D \sim$

$O(10^3)$, where $\dot{\gamma}$ is magnitude of the local shear rate), henceforth we neglect this effect. The viscosity of the suspension is a function of particle volume fraction, $\mu = \mu(\phi)$. Here, we use the expression from [27], $\mu(\phi) = \mu_l (1 - \phi/\phi_{max})^{-2}$, where ϕ_{max} denotes maximum packing volume fraction, and restricts the meaningful interval of values for ϕ to $[0, \phi_{max}]$, with the mixture becoming almost solid-like as $\phi \rightarrow \phi_{max}$. Different values of ϕ_{max} have appeared in the literature, usually within the range 0.57–0.68 (e.g. see [12, 13, 17, 19, 22, 20, 23, 26, 27]). We use the procedure described in [13] and obtain $\phi_{max} \approx 0.61$. Also, $\mu_l = \nu\rho_l$.

The settling of a particle due to gravity is hindered by the presence of other particles and the solid track/wall [10]. The net flux of particles caused by this effect is given by

$$\mathbf{J}_{grav} = -\frac{d^2\phi(\rho_p - \rho_l)}{18\mu_l} f(\phi)\omega(z)\mathbf{g}. \quad (2)$$

Here, we use the hindrance function from [20]: $f(\phi) = \mu_l(1 - \phi)/\mu(\phi)$. The presence of a solid track at $z = 0$ is taken into account through $\omega(z) = A(z/d)^2 / \sqrt{1 + A^2(z/d)^4}$ [10]; $A = 1/18$ so that $\omega(z) \rightarrow 0$ as $z \rightarrow 0$, and $\omega \approx 1$ away from $z = 0$. We note that this is the main difference between our model and the one derived in [12]: we include the hindrance $\omega(z)$ in our settling model, while in [12], this effect is neglected altogether.

The effect of shear-induced migration is included in Eq. 1 through two separate terms, \mathbf{J}_{coll} and \mathbf{J}_{visc} . These terms are defined as in [22] and [23]. The net flux of particles due to irreversibility of collisions between pairs of particles is given by

$$\mathbf{J}_{coll} = -K_{coll} \frac{d^2}{4} (\phi^2 \nabla \dot{\gamma} + \phi \dot{\gamma} \nabla \phi). \quad (3)$$

On the other hand, the net flux due to gradients in viscosity, $\mu(\phi)$, is given as

$$\mathbf{J}_{visc} = -K_{visc} \frac{d^2}{4} \phi^2 \dot{\gamma} \frac{1}{\mu(\phi)} \frac{d\mu}{d\phi} \nabla \phi. \quad (4)$$

Here, K_{coll} and K_{visc} are proportionality constants determined from experiments. We follow [23] and use $K_{coll} = 0.41$ and $K_{visc} = 0.62$.

The fluxes given in Eqs. 2, 3 and 4 are all proportional to d^2 , a fact we have employed in §3, in our argument regarding the influence of particle size on settling behavior of particles. It is interesting to note that in Eq. 3, the first term suggests that even if the particle distribution is uniform (i.e. $\nabla \phi = 0$), the migration will occur due to gradients in frequency of irreversible particle collisions. This migration will then induce gradients in ϕ and hence, the second term in Eq. 3 is activated.

The governing equation given in 1, is accompanied by boundary conditions (zero normal flux at both $z = 0$ and $z = h$, where h is film thickness) and coupled to Navier-Stokes equations for liquid with viscosity $\mu(\phi)$. However, in order to gain insight into settling behavior of particles, it is sufficient to consider Eq. 1 at steady state [12]. Assuming the thin film is flat, the steady state is achieved when fluxes given in Eqs. 2, 3 and 4 balance in z -direction

$$\mathbf{J}_{grav} + \mathbf{J}_{coll} + \mathbf{J}_{visc} = 0. \quad (5)$$

The boundary conditions are given by $\hat{\mathbf{n}} \cdot (\mathbf{J}_{grav} + \mathbf{J}_{coll} + \mathbf{J}_{visc}) = 0$ at both $z = 0$ and $z = h$. Here, $\hat{\mathbf{n}}$ is the outward-pointing unit vector in normal direction. We also assume that the flow is simple and unidirectional, so that $\dot{\gamma} = \partial u / \partial z$. Henceforth, instead of using $\dot{\gamma}$, we revert to shear stress $\sigma = \mu(\phi)\dot{\gamma}$. By scaling Eq. 5 using H as the length scale in z -direction and $\rho_l g H \sin \alpha$ as the scale for σ , and integrating once, we arrive at the following ODE

$$\left[1 + \frac{2(K_{visc} - K_{coll})}{K_{coll}} \frac{\phi}{\phi_{max} - \phi} \right] \sigma \phi' = -\sigma' \phi - \frac{2\rho_s \cot \alpha}{9K_{coll}} (1 - \phi) \bar{\omega}(z), \quad (6)$$

where $\rho_s = (\rho_p - \rho_l)/\rho_l$, and $\bar{\omega}(z)$ is the scaled version of $\omega(z)$. Since we assume that the film is flat, the pressure is hydrostatic in the suspension and the (scaled) gradient in shear stress is given as [12]

$$\sigma' = -(1 + \rho_s \phi). \quad (7)$$

By substituting the expression from Eq. 7 into 6, we obtain

$$\left[1 + \frac{2(K_{visc} - K_{coll})}{K_{coll}} \frac{\phi}{\phi_{max} - \phi} \right] \sigma \phi' = (1 + \rho_s \phi) \phi - \frac{2\rho_s \cot \alpha}{9K_{coll}} (1 - \phi) \bar{\omega}(z). \quad (8)$$

Finally, the accompanying boundary conditions are $\sigma(0) = (1 + \rho_s \phi_0)$ and $\sigma(1) = 0$ [12], which are substituted into scaled versions of no-flux boundary conditions to obtain

$$\left[1 + \frac{2(K_{visc} - K_{coll})}{K_{coll}} \frac{\phi}{\phi_{max} - \phi} \right] (1 + \rho_s \phi_0) \phi' = (1 + \rho_s \phi) \phi, \quad (9)$$

and

$$(1 + \rho_s \phi) \phi = \frac{2\rho_s \rho_l g H}{27K_{coll} \mu_l \cos \alpha} (1 - \phi), \quad (10)$$

at $z = 0$ and $z = 1$ respectively. The system of ODEs and accompanying boundary conditions given by Eqs. 7-10 may be solved numerically for $\phi(z)$ and $\sigma(z)$. The numerical solutions of this system are discussed in §5.

Before proceeding further, we note that an identical system of equations for $\phi(z)$ and $\sigma(z)$ may be obtained directly from Eq. 1 by employing scaling arguments typical to thin film flows and considering the leading order terms in $\epsilon = (3Ca)^{1/3}$, where Ca is capillary number (see Appendix for details).

5. Predictions of theoretical model vs. experimental results

The system of equations for $\phi(z)$ and $\sigma(z)$ given by 7-10 is solved using a shooting method. The shooting is carried out from $z = 0$, with $\phi(0) = 0$ adjusted in order to satisfy $\int_0^1 \phi(z) dz = \phi_0$. Since $\partial u / \partial z = \sigma(z) / \mu(\phi(z))$, once $\phi(z)$ and $\sigma(z)$ are known, $u(z)$ is readily found, by simply integrating once and using the no-slip boundary condition, $u(0) = 0$.

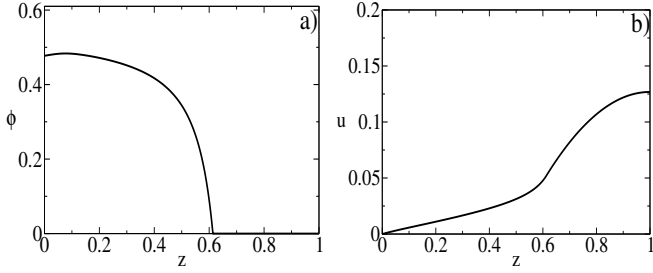


Figure 6: Numerical solution for $\phi_0 = 0.250$ and $\alpha = 15^\circ$: (a) particle volume fraction, $\phi(z)$; and (b) velocity, $u(z)$. Note that $\phi_{max} > \phi(0) > \phi_0$ and $\phi(1) = 0$. This corresponds to *settled* regime.

As previously noted in [12], due to the fact that σ is non-negative, ϕ is a monotonic function of z . This is because $\sigma\phi'$ in Eq. 8 is determined by a function of ϕ only, with a single unstable root $\bar{\phi}(\alpha)$ in the interval $[0, \phi_{max}]$. Hence, either $\phi_{max} > \phi(0) > \phi_0$ and $\phi(1) = 0$, or $\phi(0) < \phi_0$ and $\phi(1) = \phi_{max}$, corresponding to experimentally observed settled and ridged regimes respectively. The well-mixed regime occurs when $\phi' = 0$ and $\phi(z) = \phi_0$ for $0 < z < 1$. Setting $\phi' = 0$, $\phi = \phi_0$ in Eq. 8 allows us to obtain an expression for α in terms of ϕ_0

$$\alpha = \tan^{-1} \left[\frac{2\rho_s}{9K_{coll}} \frac{1 - \phi_0}{(1 + \rho_s\phi_0)\phi_0} \right]. \quad (11)$$

The curve corresponding to this expression is shown as a solid line compared with the experimental results in the phase diagrams of Figs. 3, 4 and 5. The profiles for $\phi(z)$ and $u(z)$ obtained by numerically solving Eqs. 7-10 using several representative combinations of ϕ_0 and α values are shown in Figs. 6, 7 and 8.

Figure 6 shows the profiles for $(\phi_0, \alpha) = (0.250, 15^\circ)$, corresponding to the settled regime in all phase diagrams in Figs. 3, 4 and 5. From Fig. 6a) it is evident this is the scenario where $\phi_{max} > \phi(0) > \phi_0$ and $\phi(1) = 0$. Most of the particles are in $z \leq 0.5$, after which ϕ decreases rapidly. Effectively, the particle-rich lower layer is covered by a less viscous clear liquid layer. Furthermore, in Fig. 6b), the velocity increases sharply for $z > 0.5$, causing clear liquid layer to flow faster than the particle-rich one. This is equivalent to the regime seen in Figure 2a) in which particles settled to the substrate and clear liquid continues down the track. In this case, the prediction of our model agrees well with the experimental results.

In Fig. 7, the profiles for ϕ and u resulting from $(\phi_0, \alpha) = (0.475, 45^\circ)$ are given. We note that in all our experiments with these values of ϕ_0 and α , the ridged regime occurs (see Figs. 3, 4 and 5). Figure 7a) shows, in contrast to Fig. 6a), that $\phi(0) < \phi_0$ and $\phi(1) = \phi_{max}$. Therefore, particles aggregate close to the free surface of the film, and according to Fig. 7b), flow faster than the more dilute lower layer. This behavior is typical in the ridged regime observed in experiments and the model predictions are again in good agreement with our experimental results.

Finally, for $(\phi_0, \alpha) = (0.310, 45^\circ)$, the resulting ϕ and u profiles are given in Fig. 8. With the exception of experiments with the largest particles (see Fig. 4c)), this combination of ϕ_0 and α values leads to a well-mixed regime. From Fig. 8a), we see

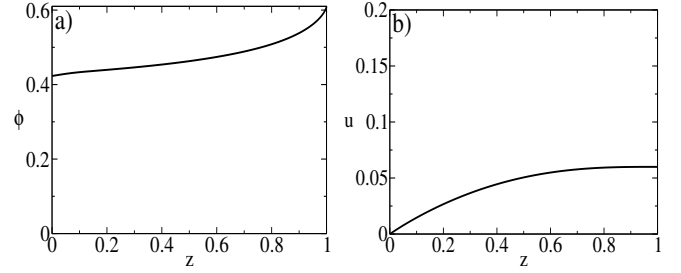


Figure 7: Numerical solution for $\phi_0 = 0.475$ and $\alpha = 45^\circ$: (a) particle volume fraction, $\phi(z)$; and (b) velocity, $u(z)$. Note that $\phi(0) < \phi_0$ and $\phi(1) = \phi_{max}$. This corresponds to *ridged* regime.

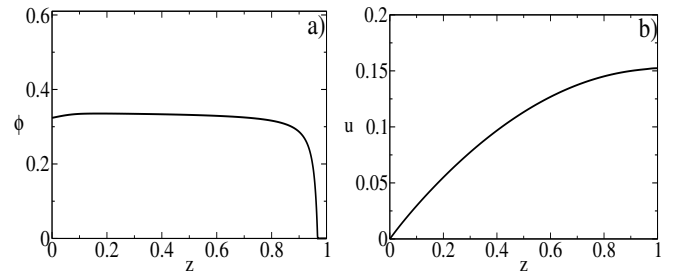


Figure 8: Numerical solution for $\phi_0 = 0.310$ and $\alpha = 45^\circ$: (a) particle volume fraction, $\phi(z)$; and (b) velocity, $u(z)$. Note that $\phi_{max} > \phi(0) > \phi_0$ and $\phi(1) = 0$ still apply.

that for most of the film thickness, the particles are uniformly distributed. However, a close inspection reveals that this case still belongs to the category of solutions to Eqs. 7-10 where $\phi_{max} > \phi(0) > \phi_0$ and $\phi(1) = 0$, namely the settled regime. In addition, Fig. 8b) indicates that the very thin layer of clear liquid at the free surface still flows faster than the particle-laden layer below it. While our model is a steady state one, one could clearly see how in a dynamic setting the situation shown in Fig. 8 eventually leads to a settled regime, with the top layer of clear liquid becoming ever thicker and flowing ever faster as the system evolves.

Next, we examine the agreement between the $\alpha(\phi_0)$ well-mixed curve given by Eq. 11, and the experimental results. We note that, apart from the inclusion of the hindrance due to the presence of a solid track in our model, another important difference between this study and the one in [12] is that we compare the predictions of our model to the results of much more extensive experiments. For this purpose, we go back to Figs. 3, 4 and 5. In all diagrams, except the one in Fig. 4c), the curve lies completely within the well-mixed band, in excellent agreement with the experimental results. For largest particles in Fig. 4c), the well-mixed regime does not occur; however, the curve overlaps a large section of the border between settled and ridged bands marking the transition between these two regimes. This again hints at the transiency of the well-mixed regime. The structure of Eqs. 7-10 also indicates that the well-mixed regime is an unstable root of the system. Even if ϕ_0 and α values are adjusted to lie exactly on the well-mixed curve, even smallest perturbations eventually cause bifurcation to either settled or ridged regime. The strongest evidence for this argument is given by Fig. 4c), where relevant settling time scales are short

enough so that bifurcation occurs rapidly and the well-mixed band simply collapses to well-mixed curve. Other phase diagrams in Figs. 3, 4 and 5 are also in line with our argument, only the time scales at which the bifurcation occurs are much longer compared to the one in Fig. 4c), leading to observable well-mixed regime. A sufficiently long experimental track would allow for bifurcation to occur, resulting in eventual collapse of all well-mixed bands in Figs. 3, 4 and 5.

Finally, it is worthwhile to emphasize that our model is a steady state one, while the behavior shown e.g. in Fig. 2a), where a clear film leaves a particle rich sediment behind and develops fingers, is clearly a dynamic process, which could only be captured by a more complete evolutionary-type model. However, the settling behavior, which our simple model correctly predicts, is the most crucial ingredient, as it truly sets the stage for these more complex dynamic processes. Therefore, our model should be considered as one of the main components of any fully dynamic model.

6. Conclusions

In this paper, we focus on experiments with particle-laden thin film flows down an incline, where the effects of the viscosity of the suspending liquid and the particle size are examined. We observe that the settling behavior of particles proceeds in three distinct regimes: settled, well-mixed, and ridged, depending on the bulk volume fraction, ϕ_0 , and the inclination angle, α . Our theoretical model, based on an equilibrium theory, where the hindered settling balances the shear-induced migration, is found to be in an excellent agreement with our experimental data. More precisely, its predictions for the transition between the settled and the ridged regime match the experimental observations exactly over all ranges of viscosities and particle sizes. Furthermore, both our model and our experimental results suggest that the intermediate well-mixed regime is a transient. In particular, our equilibrium theory predicts no such regime; our experiments show how the well-mixed band collapses as the relevant time scales are changed by varying the viscosity and the particle size. Therefore, we argue that the well-mixed regime eventually leads to a bifurcation to either the settled or the ridged regime.

Our experimental results indicate that the particle size is a significant parameter. The likelihood of observing the well-mixed regime increases with the decrease in the particle diameter. The viscosity of the suspending liquid is found to affect the relevant time scale of the flow. For the smallest considered particle size, the liquid viscosity also significantly affects the likelihood of the well-mixed regime: it is more prevalent in the case of a less viscous suspending liquid. A combination of a low viscosity liquid and small particles significantly affects the relevant time scales. The flowing film runs out of track length before any substantial disturbance to the uniformity of the suspension is observed. We argue that given a sufficiently long track, the well-mixed bands in phase diagrams such as those in Figs. 3, 4 and 5 might eventually collapse to a well-mixed line given by Eq. 11, so that only the settled and the ridged regimes are observed.

The development of a tractable theoretical model for particle-laden thin films, incorporating all the relevant physical mechanisms, is an interesting problem. This model would have to account for the momentum conservation and continuity in the liquid, and include the capillary and the contact line effects, along with those relevant to the particle migration. Hence, this task is still a formidable one. Instead, a simplified steady state model is derived here. The model considers a balance between the hindered settling and the shear-induced migration of particles, and it is shown to provide useful new information about the settling behavior. This paper therefore makes a significant step toward a fully quantitative model by identifying the dominant equilibrium physics for the flow. In addition, it also implies further modifications required in order to fully understand the transiency of the well-mixed regime and the intricacies connected to the time scales relevant to the front motion and the particle settling. Our study also raises interesting questions regarding the motion of the contact lines and the fingering instability. A more complete theoretical model would allow for a comparison with the time dependent experimental results from [13], regarding the front motion in particle-laden films. In addition, the experiments with clear liquid flows in [4] showed that once the fingering instability occurred, the exponent in the power law (e.g. see [1]) describing the evolution of the front position was modified. Carrying out a similar study in the particle-laden settling would indeed be compelling, especially since it would also allow for examination of the connection between different settling regimes and the wavelength of the fingering instability.

Acknowledgements

The authors would like to gratefully acknowledge the helpful comments of B. P. Cook. The bulk of experimental work presented here was carried out during the Research Experience for Undergraduates (REU) program at University of California, Los Angeles during Summer 2009. This work was supported by NSF (DMS-0601395), and the UC Lab research fund (09-LR-04-116741-BERA).

A. Appendix

Here, we give an alternate approach for deriving Eq. 6 (i.e. the steady state equation) directly from the dynamic equation for ϕ , Eq. 1. First, the expressions for particle fluxes due to the hindered settling and the shear-induced migration, Eqs. 2-4 are substituted into Eq. 1. Assuming $\mu(\phi)$ is given as in §4, and $\dot{\gamma} = \partial u / \partial z$, Eq. 1 becomes

$$\begin{aligned} \phi_t + u\phi_x + w\phi_z = & \frac{d^2 K_{coll}}{4} (\phi(u_z\phi)_x)_x + \\ & \frac{d^2 K_{coll}}{4} (\phi(u_z\phi)_z)_z + \\ & \frac{d^2 K_{visc}}{2\phi_{max}} \left(u_z\phi^2 \left(1 - \frac{\phi}{\phi_{max}} \right)^{-1} \phi_x \right)_x \end{aligned}$$

$$\begin{aligned} & \frac{d^2 K_{visc}}{2\phi_{max}} \left(u_z \phi^2 \left(1 - \frac{\phi}{\phi_{max}} \right)^{-1} \phi_z \right)_z + \\ & \frac{d^2 \rho_s \rho_l g \sin \alpha}{18\mu_l} \left(\phi (1 - \phi) \left(1 - \frac{\phi}{\phi_{max}} \right)^2 \omega(z) \right)_x + \\ & \frac{d^2 \rho_s \rho_l g \cos \alpha}{18\mu_l} \left(\phi (1 - \phi) \left(1 - \frac{\phi}{\phi_{max}} \right)^2 \omega(z) \right)_z, \quad (12) \end{aligned}$$

where the subscripts denote derivatives. Next, we scale Eq. 12 using the time, length, and velocity scales typically utilized for thin film flows (the lubrication approximation, e.g. see [10]). Namely, the small parameter is $\epsilon = (3Ca)^{1/3}$, where $Ca = (\rho_l g H^2 \sin \alpha) / (3\gamma)$ is the capillary number, and γ is the surface tension of the liquid. The scale in the z -direction is H , and the one in the x -direction is H/ϵ ; u is scaled using $u_{sc} = (H^2 \rho_l g \sin \alpha) / (3\mu_l)$, while w is scaled using ϵu_{sc} ; the time scale is given as $H / (\epsilon u_{sc})$. In addition, we assume that $\phi \sim \mathcal{O}(1)$. To the leading order in ϵ , we obtain

$$\begin{aligned} & K_{coll} \left(\phi (u_z \phi) \right)_z + \frac{2K_{visc}}{\phi_{max}} \left(u_z \phi^2 \left(1 - \frac{\phi}{\phi_{max}} \right)^{-1} \phi_z \right)_z + \\ & \frac{2}{3} \rho_s (\cot \alpha) \left(\phi (1 - \phi) \left(1 - \frac{\phi}{\phi_{max}} \right)^2 \bar{\omega}(z) \right)_z = 0. \quad (13) \end{aligned}$$

We proceed by substituting $u_z = 3(1 - \phi/\phi_{max})^2 \sigma$ and integrating Eq. 13 with respect to z . Finally, a simple manipulation yields Eq. 6.

References

- [1] H. Huppert, Flow and instability of a viscous current down a slope, *Nature* 300 (1982) 427.
- [2] N. Silvi, E. B. Dussan V., On the rewetting of an inclined solid surface by a liquid, *Phys. Fluids* 28 (1985) 5.
- [3] S. M. Troian, E. Herbolzheimer, S. A. Safran, J. F. Joanny, Fingering instabilities of driven spreading films, *Europhys. Lett.* 10 (1989) 25.
- [4] J. M. Jerrett, J. R. de Bruyn, Finger instability of a gravitationally driven contact line, *Phys. Fluids A* 4 (1992) 234.
- [5] L. Kondic, A. L. Bertozzi, Nonlinear dynamics and transient growth of driven contact lines, *Phys. Fluids* 11 (1999) 3560.
- [6] L. Kondic, Instability in the gravity driven flow of thin liquid films, *SIAM Review* 45 (2003) 95.
- [7] Y. Nohguchi, K. Hutter, S. B. Savage, Similarity solutions for granular avalanches of finite mass with variable bed friction, *Continuum Mech. Thermodyn.* 1 (1989) 239.
- [8] S. B. Savage, K. Hutter, The motion of a finite mass of granular material down a rough incline, *J. Fluid Mech.* 199 (1989) 177.
- [9] O. Pouliquen, J. Delour, S. B. Savage, Fingering in granular flow, *Nature* 386 (1997) 816.
- [10] J. J. Zhou, B. Dupuy, A. L. Bertozzi, A. E. Hosoi, Theory for shock dynamics in particle-laden thin films, *Phys. Rev. Lett.* 94 (2005) 117803.
- [11] B. P. Cook, A. L. Bertozzi, A. E. Hosoi, Shock solutions for particle-laden thin films, *SIAM J. Appl. Math.* 68 (2007) 760.
- [12] B. P. Cook, Theory for particle settling and shear-induced migration in thin-film liquid flow, *Phys. Rev. E* 78 (2008) 045303.
- [13] T. Ward, C. Wey, R. Glidden, A. E. Hosoi, A. L. Bertozzi, Experimental study of gravitation effects in the flow of a particle-laden thin film on an inclined plane, *Phys. Fluids* 21 (2009) 083305.
- [14] J. F. Richardson, W. N. Zaki, The sedimentation of a suspension of uniform spheres under conditions of viscous flow, *Chem. Eng. Sci.* 3 (1954) 65.

- [15] G. K. Batchelor, Sedimentation in a dilute suspension of spheres, *J. Fluid Mech.* 52 (1972) 245.
- [16] E. Barnea, J. Mizrahi, A generalized approach to the fluid dynamics of particulate systems I. General correlation for fluidization and sedimentation in solid multiparticle systems, *Chem. Eng. J.* 5 (1973) 171.
- [17] R. Buscall, J. W. Goodwin, R. H. Ottewill, T. F. Tadros, The settling of particles through Newtonian and non-Newtonian media, *J. Colloid Interface Sci.* 85 (1982) 78.
- [18] R. H. Davis, A. Acrivos, Sedimentation of noncolloidal particles at low Reynolds-numbers, *Ann. Rev. Fluid Mech.* 17 (1985) 91.
- [19] P. Snabre, P. Mills, Settling and fluidization of non-Brownian hard spheres in a viscous liquid, *Euro. Phys. J. E* 1 (2000) 105.
- [20] U. Schaffinger, A. Acrivos, K. Zhang, Viscous resuspension of a sediment within a laminar and stratified flow, *Int. J. Multiphase Flow* 16 (1990) 567.
- [21] D. Leighton, A. Acrivos, Measurement of shear-induced self-diffusion in concentrated suspensions of spheres, *J. Fluid Mech.* 177 (1987) 109.
- [22] D. Leighton, A. Acrivos, The shear-induced migration of particles in concentrated suspensions, *J. Fluid Mech.* 181 (1987) 415.
- [23] R. J. Phillips, R. C. Armstrong, R. A. Brown, A. L. Graham, J. R. Abbott, A constitutive equation for concentrated suspensions that accounts for shear-induced particle migration, *Phys. Fluids A* 4 (1992) 30.
- [24] J. M. Kim, S. G. Lee, C. Kim, Numerical simulations of particle migration in suspension flows: Frame-invariant formulation of curvature-induced migration, *J. Non-Newtonian Fluid Mech.* 150 (2008) 162.
- [25] P. R. Nott, J. F. Brady, Pressure-driven flow of suspensions - simulation and theory, *J. Fluid Mech.* 275 (1994) 157.
- [26] J. F. Morris, F. Boulay, Curvilinear flows of noncolloidal suspensions: The role of normal stresses, *J. Rheology* 43 (1999) 1213.
- [27] B. D. Timberlake, J. F. Morris, Particle migration and free-surface topography in inclined plane flow of a suspension, *J. Fluid Mech.* 538 (2005) 309.